RESEARCH ARTICLE
SPACE PHYSICS: IONOSPHERIC PHYSICS

Earth and Planetary Physics
7: 460–470, 2023
doi: 10.26464/epp2023047

Development of a low-frequency magnetic lightning mapping system (LFM-LMS) in North China: validation and preliminary results

Xiao Li[1], GaoPeng Lu[1,2,3*], FanChao Lyu[4], HongBo Zhang[5], Kainat Qamar[1], and RuBin Jiang[5]

[1]School of Earth and Space Sciences, University of Science and Technology of China, Hefei 230026, China;

[2]Key Laboratory of Atmospheric Optics, Anhui Institute of Optics and Fine Mechanics, HFIPS, Chinese Academy of Sciences, Hefei 230031, China;

[3]Collaborative Innovation Center on Forecast and Evaluation of Meteorological Disasters, Nanjing University of Information Science & Technology, Nanjing 210044, China;

[4]Key Laboratory of Transportation Meteorology of China Meteorological Administration, Nanjing Joint Institute for Atmospheric Sciences, Nanjing 210000, China;

[5]Key Laboratory for Middle Atmosphere and Global Environment Observation, Institute of Atmospheric Physics, Chinese Academy of Sciences, Beijing 100029, China

Key Points:

- A low-frequency magnetic lightning mapping system (LFM-LMS) was developed during the SHAndong Triggered Lightning Experiment, North China.
- The location accuracy of LFM-LMS was estimated to be about 100–200 m horizontally and ~200 m vertically with the rocket triggered lightning.
- The LFM-LMS can reconstruct the 3D morphology of lightning, with well-defined propagation paths of negative leaders.

Citation: Li, X., Lu, G. P., Lyu, F. C., Zhang, H. B., Qamar, K., and Jiang, R. B. (2023). Development of a low-frequency magnetic lightning mapping system (LFM-LMS) in North China: validation and preliminary results. *Earth Planet. Phys.*, *7*(4), 460–470. http://doi.org/10.26464/epp2023047

Abstract: A low-frequency magnetic lightning mapping system (LFM-LMS) was built during the SHAndong Triggered Lightning Experiment (SHATLE), based on continuous measurements of magnetic field radiation from lightning. The hardware and source-mapping techniques used by the LFM-LMS were introduced; both Monte Carlo simulations and the observation of rocket-triggered lightning examples were employed to examine the location accuracy and detection effectiveness of the LFM-LMS. We estimated that the system's location accuracy about 100–200 m horizontally and ~200 m vertically. A natural intra-cloud lightning flash and a rocket-triggered lightning flash, both with intricate structures and discharging processes, were examined using the three-dimensional mapping results. The progressing path of negative lightning leaders is usually well-defined, and its propagation speed is estimated to be (0.5–1.4) × 10^6 m/s. In summary, the LFM-LMS can reconstruct the three-dimensional morphology of lightning flashes; this technology provides a efficient method for investigating the characteristics of lightning development, as well as the overall electrical strucuture of thunderstorms.

Keywords: rocket-triggered lightning; low-frequency magnetic field; lightning mapping observation; location accuracy

1. Introduction

Lightning mapping is an important and effective method to obtain key morphological features of lightning flashes. Researchers have developed many lightning location systems, operating in various frequency bands, since different ranges of electromagnetic wave frequencies correspond to different discharging behaviors during lightning events (Rakov and Uman, 2003). The very high-frequency (VHF) lightning mapping technique was first used to image intra-cloud (IC) and cloud-to-ground (CG) lightning flashes by computing differences in time-of-arrival (TOA) associated with specific breakdown sources (Proctor, 1981; Proctor et al., 1988). Subsequently, more lightning location systems focused on the VHF range were developed to reconstruct the lightning channel in two-dimensional (2D) space (Rhodes et al., 1994; Shao XM et al., 1995; Shao and Krehbiel, 1996; Stock et al., 2014) or three-dimensional (3D) space (Rison et al., 1999; Thomas et al., 2004; Zhang GS et al., 2015; Hare et al., 2018; Liu B et al., 2020; Yang QL et al., 2021).

More recently, lightning location systems in the very low-

First author: X. Li, iaplix8@ustc.edu.cn
Correspondence to: G. P. Lu, gaopenglu@gmail.com
Received 28 NOV 2022; Accepted 09 MAY 2023.
Accepted article online 07 JUN 2023.

frequency and low frequency (VLF/LF) bands have been significantly improved — from 2D locations of relatively intense discharges (Cummins et al., 1998; Smith et al., 2004) to 3D structures of large-scale discharging processes, and even to detailed morphology of a lightning flash. A VLF/LF lightning location system is constructed by installing several sensors, on a baseline in the range of 10–20 km, to record the lightning electric field (*E*-field) change pulses at multiple locations (Bitzer et al., 2013; Karunarathne et al., 2013; Wang Y et al., 2016; Shi DD et al., 2017; Wu T et al., 2018; Fan XP et al., 2018; Chen ZF et al., 2019; Yuan SF et al., 2020; Ma ZL et al., 2021) or LF magnetic field signals (Lyu FC et al., 2014, 2016). Specifically, Cummins et al. (1998) and Smith et al. (2002) reported the 2D locations of strong lightning events with LF *E*-field change sensors; such location results are conducive to tracking the evolution of thunderstorms. However, 3D location technique is required if more information about lightning morphology is to be obtained, such as the lightning's horizontal and vertical scales, inception position, channel development, and thunderstorm charge structures. Bitzer et al. (2013) used a VLF/LF *E*-field change measurement system to obtain 3D positions of radiation sources. Yoshida et al. (2014) performed 3D mapping in Japan to image structural details of lightning, including preliminary breakdown (PB), negative leaders, CG strokes, and attempted leaders. Wang Y et al. (2016) developed a VLF/LF 3D lightning location network (BLNET) in the Beijing region. Later, Yuan SF et al. (2020) used BLNET to reveal the origin of a multi-stroke positive CG lightning with different termination points. Ma ZL et al. (2021) reported their lightning location network with *E*-field change measurement during the SHATLE experiment. Shi DD et al. (2017) reported an LF *E*-field detection array (LFEDA) at the Lightning Field Experiment Base in Guangzhou, and analyzed the development of lightning through the mapping of discharge channels. Later, Fan XP et al. (2018) and Chen ZF et al. (2019) improved the performance of the LFEDA by pre-processing the LF *E*-field change signals with different methods to optimize the location algorithm, such as empirical mode decomposition and time reversal. The lightning location systems mentioned above are all operated with *E*-field change signals.

Meanwhile, the 3D lightning mapping was also reported with LF magnetic field measurement. Lyu FC et al. (2014, 2016) reported studies of total lightning positioning that employed an LF near-field interferometric-TOA 3D Lightning Mapping Array (LFI-LMA), which made continuous measurement of the magnetic field using orthogonal coils focused on the low frequency band. The discharge position corresponding to the magnetic pulse was determined by searching searching in a pre-built 3D grid according to the time-of-arrival differences at different stations, found by a cross-correlation algorithm. The LFI-LMA provided a clear view of the dynamic development of lightning leaders; this technique can also contribute to the study of initiation mechanisms of upward positive flashes (Lyu FC et al., 2021).

The performance of lightning location systems in LF/VLF bands has been improved dramatically over the years, significantly facilitating studies of the temporal evolution and spatial expansion of lightning flashes, especially research of cloud-to-ground (CG) lightning that produces transient luminous events (TLEs) in the middle and upper atmosphere (e.g. Wang YP et al., 2019) or causes whistlers and tweeks in the Earth-ionospheric waveguide (Yi J et al., 2020).

In this paper, we report measurements performed during the summer campaign of the SHAndong Triggered Lightning Experiment (SHATLE) (Qie XS et al., 2010). A low-frequency lightning location network operating with low-frequency magnetic field sensors was deployed in Binzhou City, Shandong Province, to image the 3D morphology of lightning discharges. In particular, we examined, with multi-disciplinary measurement, the 3D structure of one triggered bipolar lightning flash (which transferred both negative and positive charge from thundercloud to the ground), and one natural intra-cloud lightning flash. Below we examine the 3D imaging results and the charge transfer associated with specific discharging processes, in conjunction with other measurements during the flashes, such as the channel-base current, surface *E*-field change.

2. Description of the Network

2.1 Layout and Instrumentation of LFM-LMS

Since the summer season of 2015, a low-frequency magnetic lightning mapping system (LFM-LMS) has been developed in the SHAndong Triggered Lightning Experiment (SHATLE) in Binzhou City, Shandong Province (Qie XS et al., 2010). As shown in Figure 1, LFM-LMS consisted originally of six low-frequency (LF) magnetic field detectors; it was upgraded to seven stations in 2019, with a baseline range of 10 to 18 km. JIUS station is about 1 km from the rocket launch site (37.82°N, 118.11°E). All the other stations are deployed within 10 km around the rocket launch site, The present station deployment is as described by Ma ZL et al. (2021); however, the 3D lightning mapping network introduced by Ma ZL et al. (2021) was based on the measurement of the *E*-field change made with plate antennae.

Each station contains a set of LF magnetic sensors with two orthogonal coils and an amplifier, a computer with data acquisition module, and a GPS receiver for synchronization (with time accuracy better than 25 ns). All sensors have the same bandwidth (30–500 kHz) and gain (0.4 V/nT). The magnetic signal detected by sensor

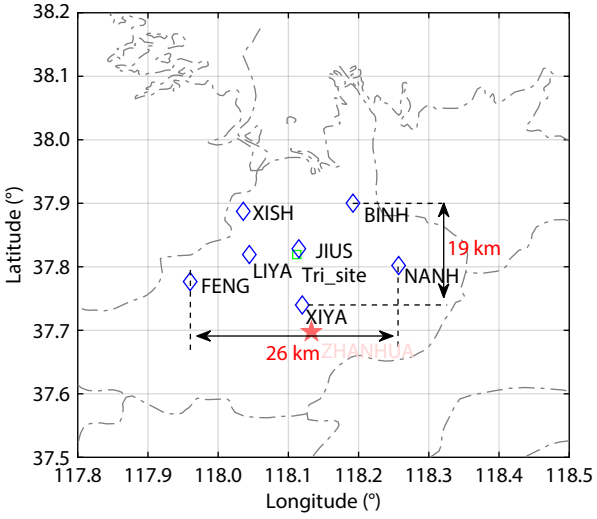

Figure 1. Layout of the low-frequency (LF) magnetic lightning location array during the SHAndong Triggered Lightning Experiment (SHATLE) in Binzhou City, Shandong Province.

is transmitted by the coaxial cable to the acquisition system and is recorded continuously at the sampling rate of 1 MSa/s (1 million sampling points per second). All the station are synchronized by GPS receiver of the same model.

2.2 Location Algorithm of LFM-LMS

The LFM-LMS is designed to image the detailed 3D structure of lightning flashes that are hidden deep inside a thundercloud. The mapping process of the LFM-LMS has two main parts: one is the determination of the time difference of arrival of signal at different stations, which tests for a possible common LF-signal source; the second part is the positioning procedure. The following two-step parsing was applied to search the continuously recorded signals for discharging events of interest.

(1) Step 1: Cross-correlation was used in a 350 μs sliding window to find the average time lags (named the 1st time lags) of the signals in the window; this is the same as the method described by Lyu FC et al. (2014, 2016). Then, the signals from paired stations are shifted according to the 1st time lags.

(2) Step 2: The pulse-peak finding method (for waveforms with a discernible isolated pulses) and the cross-correlation method (for waveforms with continuous changes) were further applied to compute the 2nd time lags, based on the characteristics of the signal waveform in the shifted window. The final TDOAs were determined from the time lags derived from both the 1st and 2nd rounds of processing.

Sliding to the next time window by a short step (typically 200 μs), the steps above are applied to determine the time lags of the pulses in the shifted window, and these steps are repeated until all signals are processed. Note that the length of the time window should be longer, by at least a factor of 2, than the maximum time difference between each pair of stations, but not so long that there are too many pulses. The choices of a 350 μs window length and a sliding step of 200 μs are found to be effective.

In the source positioning procedure, three-level nested grids are applied to search step by step for the optimal position of the lightning source. The ideal time difference of each grid is calculated and stored in a database. The resolution of the primary gird is set to 1.0 km within space grid volumes of 30 km × 30 km × 18 km; the optimal position is selected by the criterion of chi-square < 10 (see Equation (1), χ^2 is used to show the goodness of the fitting between the ideal time difference and TDOAs). The resolution of the secondary grid is set to 0.3 km in the range of 1.5 km × 1.5 km × 1.5 km of space, and the optimal position is selected by the criterion of chi-square < 1. The resolution of the tertiary grid is set to 30 m in the range of 450 m × 450 m × 450 m of space, and here again the optimal position is selected by the minimum chi-square among the tertiary grid units. In this work, chi-square is calculated by the following equation:

$$\chi^2 = \frac{\sum (\Delta T_i - \Delta t_{pi})^2}{(N-1)\tau^2}, \quad (N = 1, 2, \cdots, N-1), \tag{1}$$

where, ΔT_i is the time difference from the database, Δt_{pi} is the time difference from measurements (TDOAs), N is the number of sensors, and τ is the typical time accuracy, which is determined from the distribution of the residual value of time differences between database and the calculations (TDOAs) ($\tau \sim \sqrt{(\Delta T_i - \Delta t_{pi})^2}$). Based on the analysis, nearly 80% of all points corresponds to $\tau < 0.5$ ms (with spatial accuracy of 150 m). Thus, the time accuracy of 0.5 ms is assumed in our system, and only the points with chi-square less than 1 reliable sources (Lyu FC et al., 2014; Yoshida et al., 2014). This method was referred to the work by Lyu FC et al., (2014) and Yoshida et al. (2014). A detailed flow chart of the lightning mapping process is shown in Figure 2.

The waveforms recorded at five or more stations could be used to satisfy the location requirements. However, when the number of stations involved in the time lag calculation is more than 5, time errors in the data may increase the risk of deviation in the positioning calculation procedure. In order to avoid such errors while making full use of the best signal information, when an event is recorded at more than five stations ($N > 5$), we process TDOA data from all possible combinations of five stations. Thus, the number of combination results $\boldsymbol{R}_{nc}$ will be expressed as follows:

$$\boldsymbol{R}_{nc} = C_{N-1}^{4} + C_{N-1}^{5} + 1 \quad (N = 6, 7, 8). \tag{2}$$

Then, for all combinations of stations, the location results $\{\boldsymbol{Lc}\}_i$ are found by computing the minimum $\boldsymbol{\chi}^2$ on arrival times between the pre-calculated time difference in the database and the location results of each combination of TDOAs, which can be expressed as the formula:

$$\{\boldsymbol{Lc}\}_i = \left[\boldsymbol{\chi}_i^2 \;\; \boldsymbol{X}_i \;\; \boldsymbol{Y}_i \;\; \boldsymbol{Z}_i\right]_{R_{nc}}. \tag{3}$$

Finally, the source location $\boldsymbol{L}_i$ will be determined by the following expression:

$$\boldsymbol{L}_i = [\,X \;\; Y \;\; Z\,]_i = \begin{cases} \{\boldsymbol{Lc}\}_i|_{\min(\chi^2)} = [\,\boldsymbol{X}_i|_{\min(\chi^2)} \;\; \boldsymbol{Y}_i|_{\min(\chi^2)} \;\; \boldsymbol{Z}_i|_{\min(\chi^2)}\,] & N = 5, 6, \\ \text{mean}\left(\{\boldsymbol{Lc}\}_i|_{R_{nc}-2}\right) = \begin{bmatrix} \text{mean}\,(\text{sum}\,(\boldsymbol{X}) - \max(\boldsymbol{X}) - \min(\boldsymbol{X}))|_{R_{nc}-2} \\ \text{mean}\,(\text{sum}\,(\boldsymbol{Y}) - \max(\boldsymbol{Y}) - \min(\boldsymbol{Y}))|_{R_{nc}-2} \\ \text{mean}\,(\text{sum}\,(\boldsymbol{Z}) - \max(\boldsymbol{Z}) - \min(\boldsymbol{Z}))|_{R_{nc}-2} \end{bmatrix} & N \geq 7, \end{cases} \tag{4}$$

where $\boldsymbol{R}_{nc}$ denotes the number of combinations, X, Y, Z are the coordinates of the location points, and i is the sequence number of the lightning event.

3. Performance Evaluation of LFM-LMS

3.1 Validation with the Monte Carlo Method

A popular way to evaluate the performance of systems such as our lightning location system is based on simulation with the Monte Carlo method (Koshak et al., 2004; Ma ZL et al., 2021). We have used such a method, as follows. A region centered on the position of the JIUS station (the centroid of the mapping array) is chosen to extend out +30 km and −30 km in two orthogonal directions; it is then partitioned into 3,761 pieces 1 km × 1 km sub-regions, each of which can be tested for an event's location. Tests

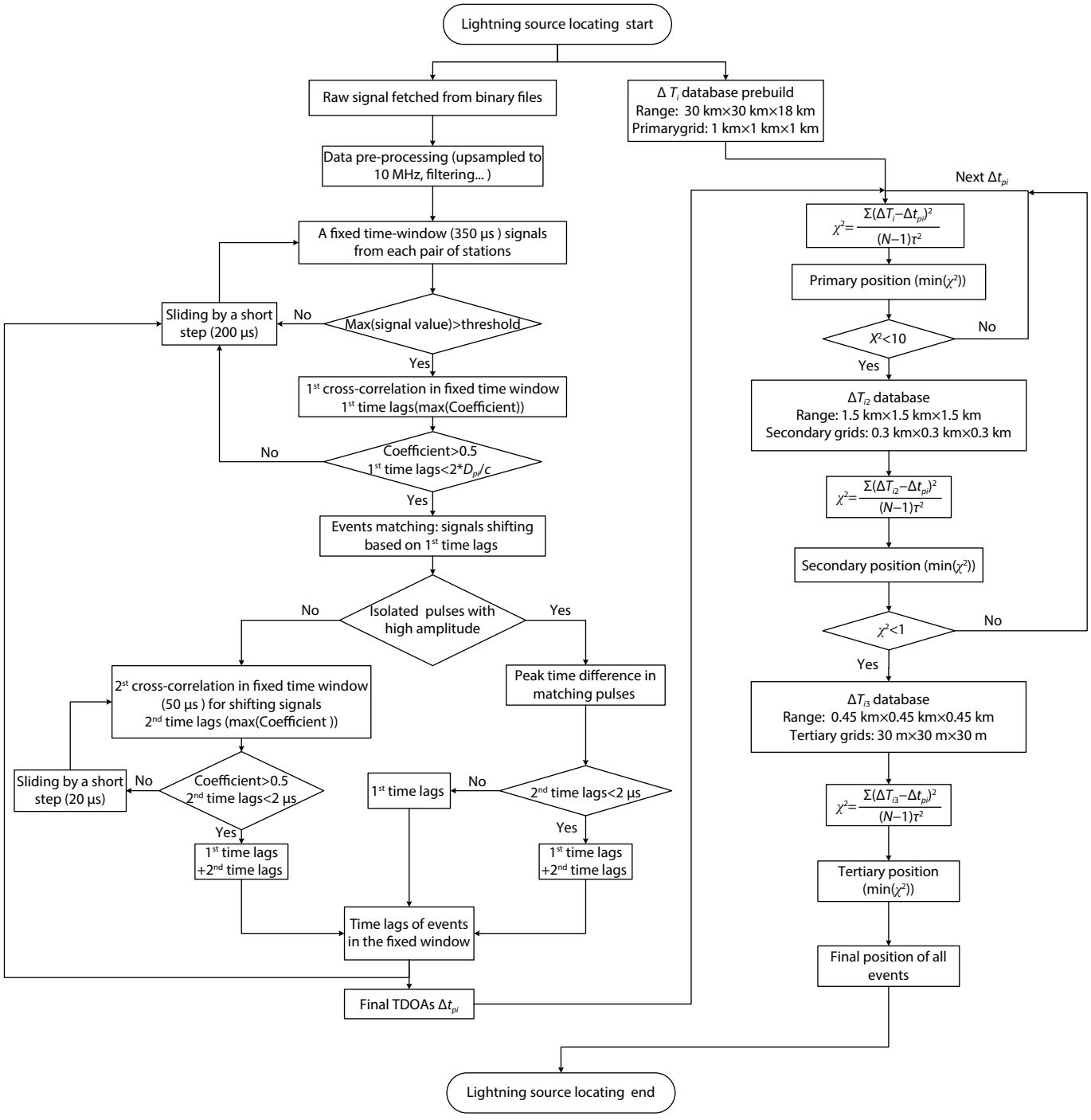

Figure 2. Flow chart of the lightning mapping process.

are performed 200 times for each grid, and each grid's final error is computed by averaging the 200 test results.

In detail, the simulation is performed in four steps: (1) expected arrival times between each sub-region $(X_{\text{original}}\ \ Y_{\text{original}}\ \ Z_{\text{original}})$ and each station are generated theoretically; (2) added to these expected arrival times is a range of timing error (noise) that follows a Gaussian distribution with a mean of 0 μs and a root-mean-square (RMS) error of 0.1 μs; the result is a range of possible TDOAs, given the specified timing-noise; (3) the sub-region position for a given event is retrieved $(X_{\text{retrieved}}\ \ Y_{\text{retrieved}}\ \ Z_{\text{retrieved}})$ by searching the database mentioned in Section 2.2; (4) the location error for each grid is computed between the known position and the retrieved position. (Note: in Step 1, the effects on signal propagation of the Earth's curvature and atmospheric disturbance on signal propagation are ignored when we determine the arrival time.) In Step 4, the error is defined by the following formulas:

for the horizontal error:

$$E_{XY} = \sqrt{(X_{\text{retrieved}} - X_{\text{original}})^2 + (Y_{\text{retrieved}} - Y_{\text{original}})^2}, \tag{5}$$

for the vertical error:

$$E_z = \left|Z_{\text{retrieved}} - Z_{\text{original}}\right|. \quad (6)$$

We replicated the operations at heights of 5 km, 10 km, and 15 km, adding to each error noise with 0 mean and RMS of 0.1, 0.2, and 0.3 μs, respectively. The simulation results are that both the horizontal and vertical errors are, on average, less than 200 m within the area (20 km × 20 km) covered by this lightning location system when the minimum time error is set to 100 ns (Figure 3 and Figure 4). As the time error is allowed to increase, the location errors are significantly enlarged, as expected, but for a given time error, the distribution of the error does not change dramatically by the change in location attitude (5, 10, and 15 km). Thus, we can

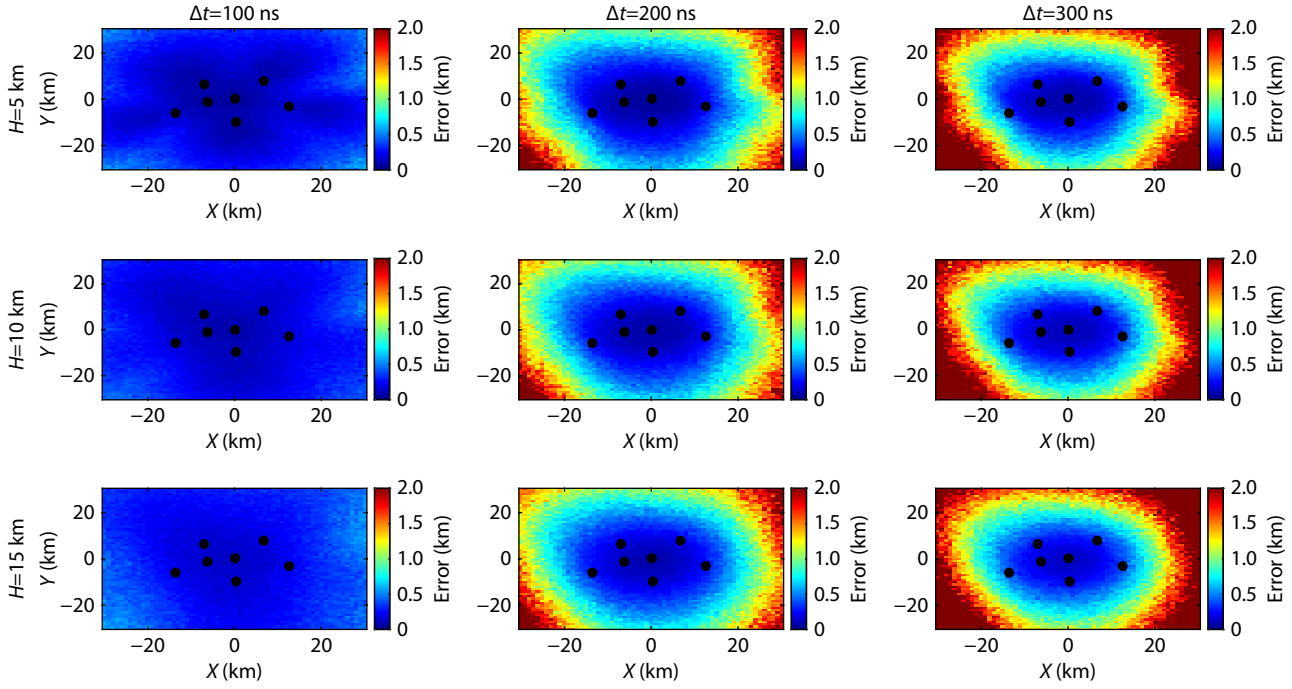

Figure 3. Planar position horizontal deviation distribution of LFM-LMS at different heights (5 km, 10 km, 15 km) with different time errors (100 ns, 200 ns, 300 ns) based on the Monte Carlo method. Black solid circles represent the geographic locations of the stations. *X* denotes the direction from West to East; *Y* denotes the direction from South to North.

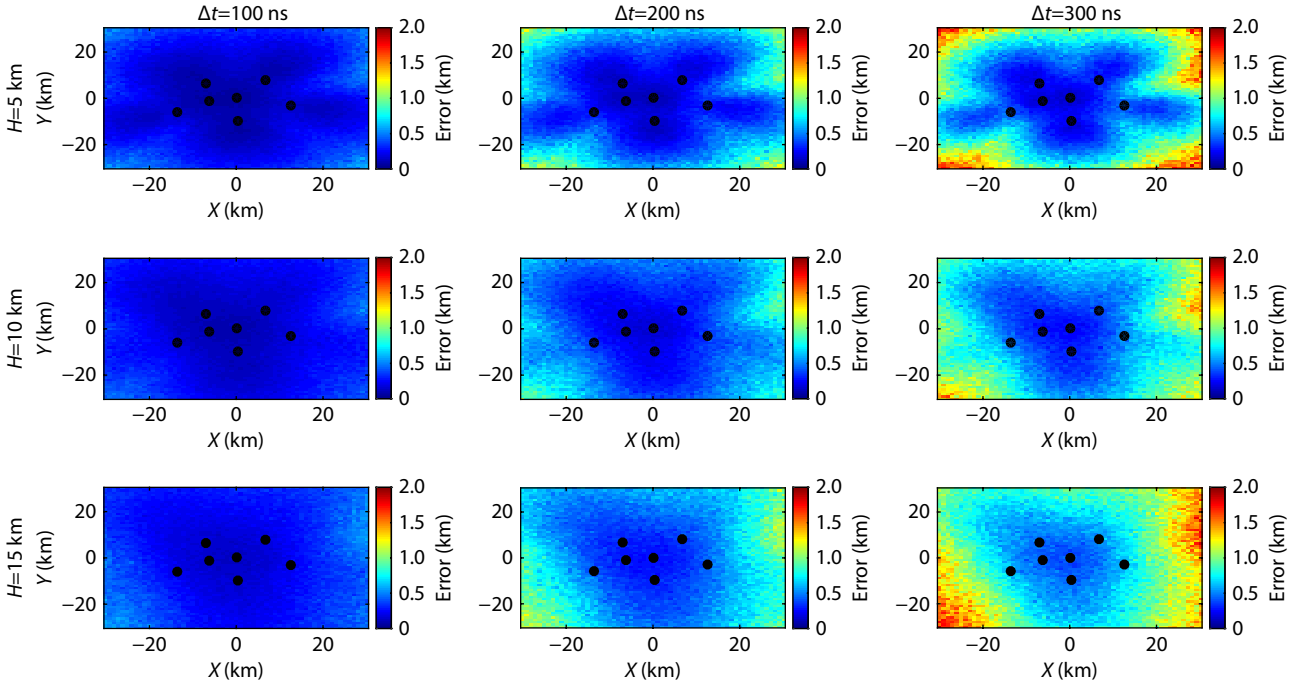

Figure 4. Planar position vertical deviation distribution of LFM-LMS at different heights (5 km, 10 km, 15 km) with different time errors (100 ns, 200 ns, 300 ns) based on the Monte Carlo method.

conclude that location accuracy is sensitive to the time difference but insensitive to event height. Compared to the findings of Ma ZL et al.(2021), our simulation was within a smaller range divided into smaller grids by considering different time errors; in addition, there are some differences between our location accuracy distribution and theirs, because we considered 7 stations (station XIAW is excluded from our analysis) whereas Ma ZL et al.(2021) simulated 8 stations.

3.2 LFM-LMS Performance Evaluation with Rocket-Triggered Lightning

During the rocket-triggered lightning experiment, multi-station sensors at varied ranges captured the synchronized magnetic waveforms of the upward leader pulses corresponding to the initial discharges during the initial stage of rocket-triggered lightning (as shown in Figure 5a); these discharges occurred at an altitude of roughly 200–400 m above the triggering site. The intensity of the initial magnetic field pulses recorded by sensors is normalized based on the amplitude of the corresponding pulse provided by the sensor at the main observation site (1.04 km from the rocket triggering site), and the relative intensity of the magnetic field pulses at various distances is calculated (as shown in Figure 5b). When fitted with inverse proportional function, the magnetic field intensity is shown to decline with distance, with a coefficient as high as 0.99.

The initial discharge position could be located using LFM-LMS. Meanwhile, other devices, such as high-speed video (HSV) and low-light-level cameras, could also give the appropriate discharge height over the triggering site. Therefore, the location accuracy of our mapping network could be determined by comparing the initial discharge position as located by LFM-LMS to the discharge height above the triggering site known from the HSV and low-light-level camera record. Upward leaders from ten triggered lightning cases were examined here, and a total of 100 pulses were extracted to be positioned by LFM-LMS. Specifically, the mean horizontal error is estimated to be 154 m by comparing the projection of the positioning points on the ground (the gray dots shown in the subplot in Figure 5c) to the triggering site position. The vertical error is estimated to be 205 m by the difference between the altitude of positioning points and the onset height of the upward leader from HSV observation (the purple line and the red line in the subplot in Figure 5d). Overall, such a positioning accuracy seems not very desirable as a positioning means to achieve a fine depiction of the 3D morphology of lightning. For the initial upward leader of the lightning initiation discharge process, the radiation source occurs at a lower height, so that the signal is easily disturbed by highly convex objects on the ground in its propagation path, resulting in a slight deviation in the arrival

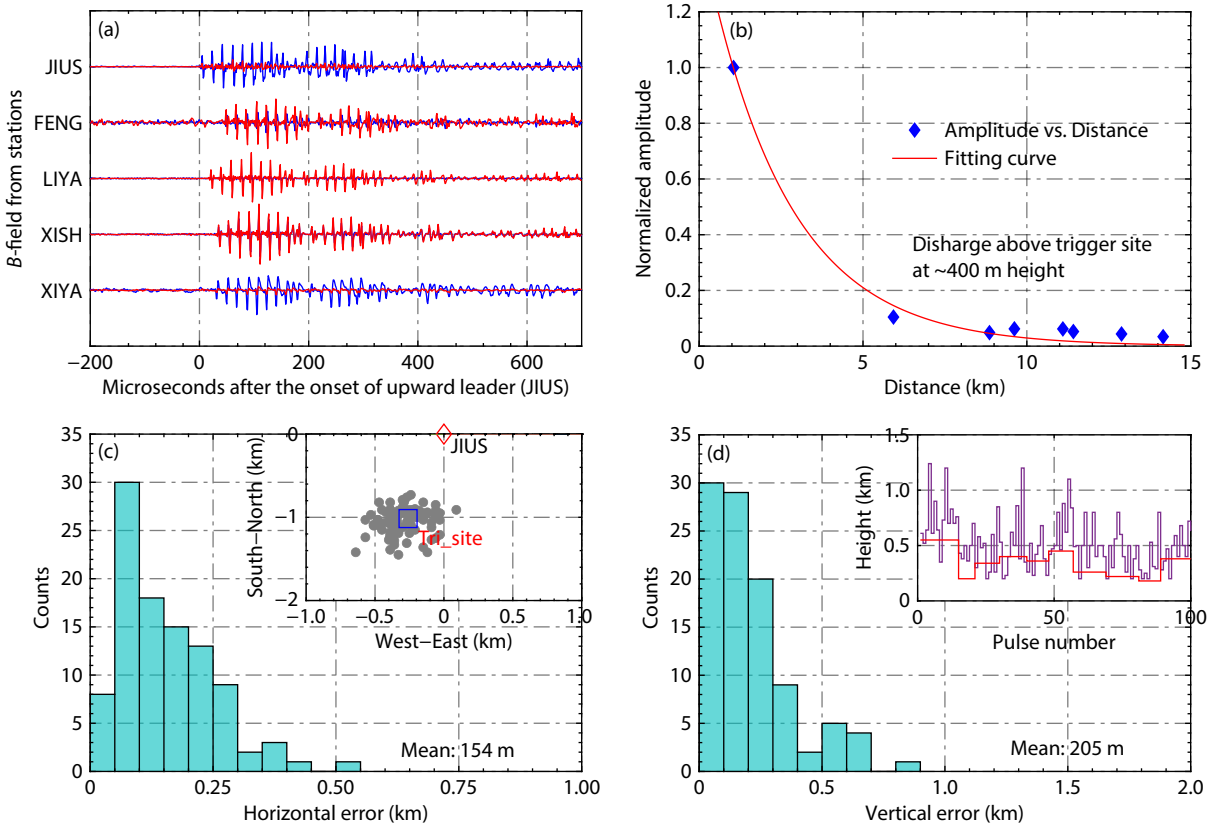

Figure 5. (a) Synchronous magnetic field signals from multiple stations during the upward leader pulse of a triggered lightning case. (b) Dependence on the amplitude of magnetic field and the distance from the source. (c) shows the horizontal error distribution and (d) shows the vertical error distribution of LFM-LMS. The gray dots shown in the subplot in (c) are the locations of initial leader pulses from several rocket triggered lightning cases. The purple line and the red line in the sub plot in (d) denote the located height of the points and the onset height of the initial upward leader, respectively.

time at the station. Theoretical simulations and analysis suggest that the accuracy of the positioning results is very sensitive to the accuracy of the pulse arrival time difference. Therefore, the estimated positioning error at a lower height should be relatively large, and the actual positioning error of the process within the cloud should be smaller than this estimate.

4. Applications of LFM-LMS

In this section, we examine the 3D mapping results of LFM-LMS during SHATLE to demonstrate the applications of this technique to study the in-cloud morphology involved in several lightning flashes of particular interests.

4.1 Mapping Results of a Bipolar Rocket-Triggered Lightning Flash

The bipolar lightning flash was triggered at 15:47:36 UTC on 14 August 2015. The channel-base current is measured directly by a 0.5 mΩ shunt with a bandwidth of 0–3.2 MHz, and the associated charge transfer is calculated (as shown in Figure 6a). Figure 5b shows the magnetic field signals measured at 970 m. The 3D

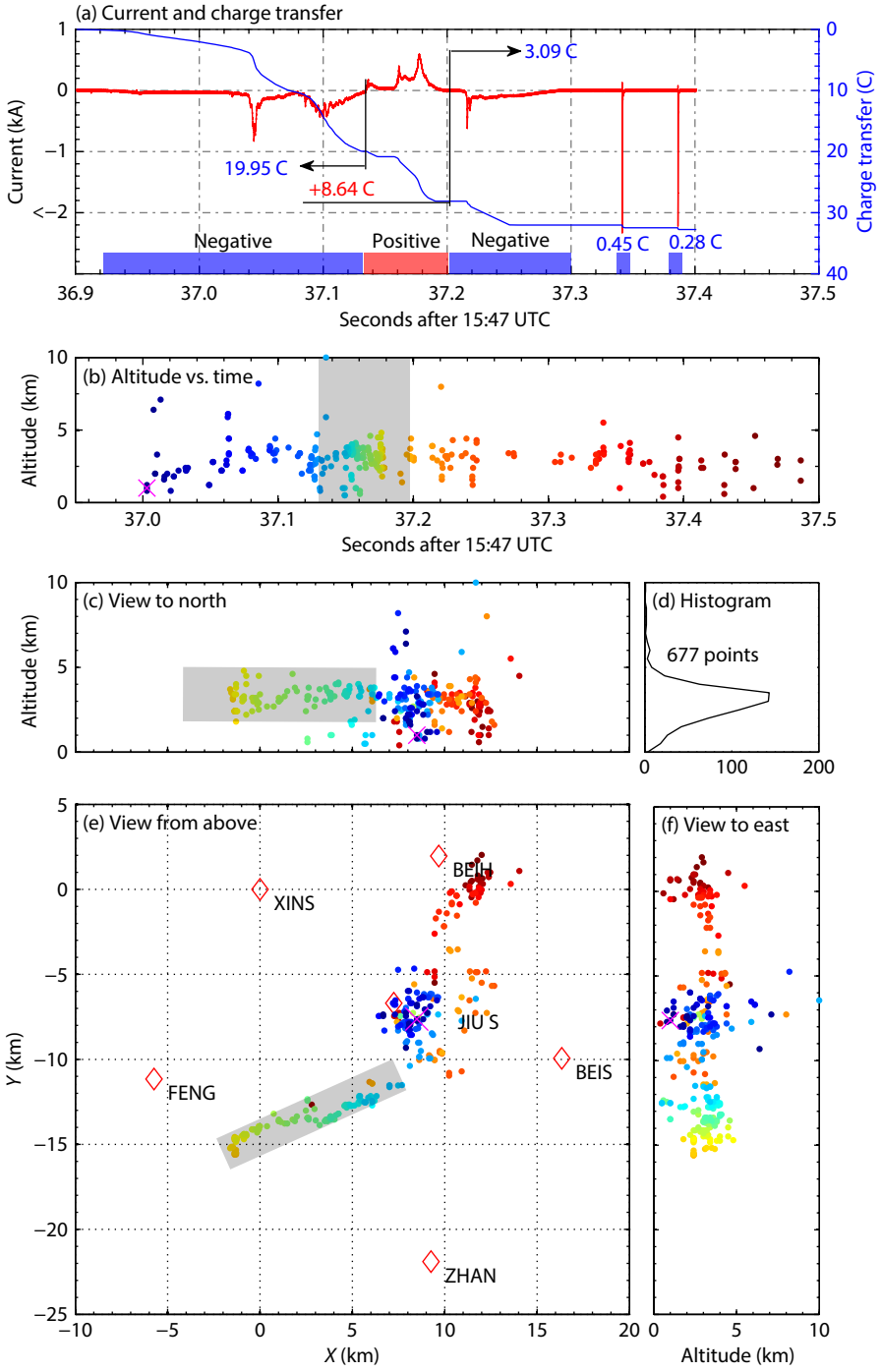

Figure 6. Charge transfer and the 3D location result of the triggered bipolar lightning. The red diamonds indicate the stations of LFM_LMS. The purple cross indicates the first located source. The colors from blue to red indicate the time variation from the beginning to the end.

structure of this bipolar rocket-triggered flash is shown in Figure 6.

The bipolar lightning was triggered by an upward positive leader (UPL), and by responding to each pulse of the upward positive leader, negative charge was transferred intermittently to the ground. As the UPL propagates upward into the thundercloud, the amplitude of the channel-base current increases until the wire is melted. The negative current lasted about 222 ms and about 19.95 Coulomb (C) negative charge was transferred to the ground. The sources of the lightning discharge were mainly located at about 2–4 km height above the triggering site. Subsequently, the polarity of the current reversed to positive immediately, which means an equivalent positive charge was transferred to the ground. Totally, about 8.64 C of charge transfer was lowered to the ground within 73.6 ms. Correspondingly, the negative leaders were identified to be more convergent in the south–west area of the thundercloud and the main channel extends about 7.5 km away at an altitude of 3–4 km with the an estimated propagation speed of 6.67×10^6 m/s. Li FQ et al. (2021) reported their mapping results, based on VHF interferometer measurements, that the negative leader channel propagates with elevation varying from 60 degrees to 10 degrees at the azimuth range of 150 degrees to 220 degrees. After that, the channel-base current decayed to zero until a negative pulse with an amplitude of about 500 A appeared and the current polarity changed from positive back to negative again. The continuous current transferred about 3.09 C of negative charge within 182.9 ms, followed by two negative dart-leader strokes with peak currents of 9.23 kA and 5.87 kA, respectively. The location results show that the charge transfer during this stage is mainly from the northeast area. Also, the LFM-LMS facilitates researches on the link between the thundercloud and the lightning morphology. Li FQ et al. (2021) have superimposed the LFM-LMS location points in the plane view on the radar echoes, which shows that the positive charge transfer process occurred in the transition zone between the convective region and the stratiform region, with radar reflectivity ranging between about 30 and 40 dBZ, and the negative charge transfer for continuous current and strokes is from the cloud area with weak echo reflectivity.

4.2 Mapping Results of a Natural Intra-cloud Lightning Flash

A natural intra-cloud lightning flash, which occurred at 22:38:16.22 UTC on July 13, 2019, was imaged by LFM-LMS, and the three-dimensional locations are shown in Figure 7. The waveform of the magnetic field at JIUS station and *E*-field change at LIYA station are shown in Figure 7a along with the temporal variation of the discharge altitude. The *S*-band weather radar located in Binzhou, about 55 km away from the SHATLE, provided the reflectivity profile of the thunderstorm, which is in the mature phase. The reflectivity at 22:36 UTC (about 2 minutes before the lightning onset) overlapped with the lightning radiation sources, as shown in Figure 8.

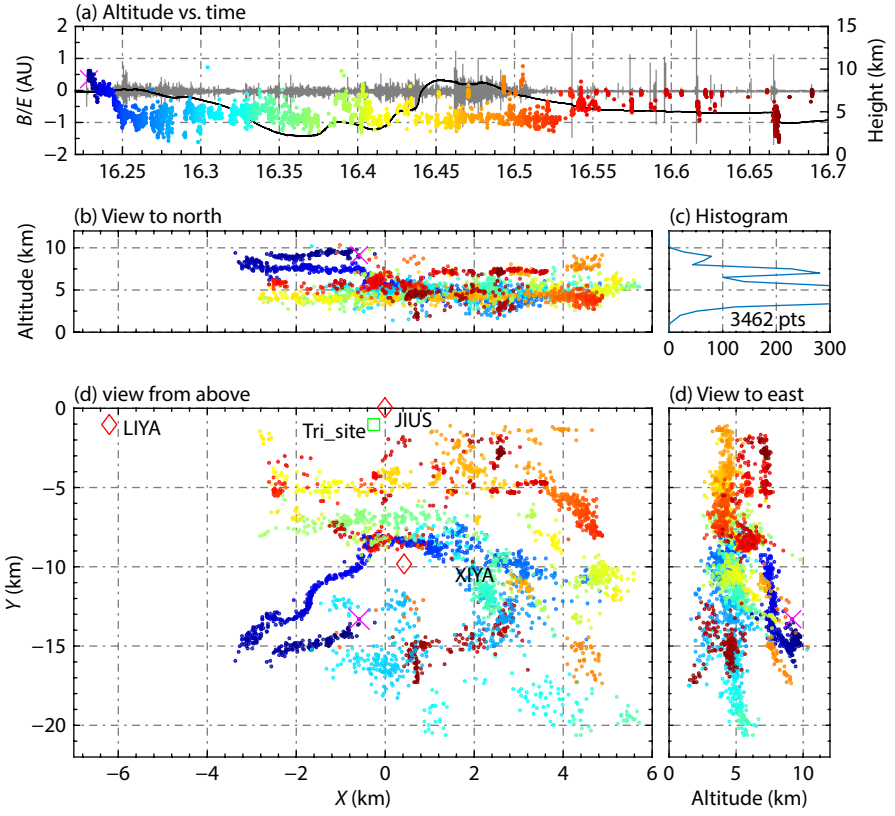

Figure 7. Three-dimensional locations of the IC flash that occurred at 22:38:16.22 (UTC) on July 13, 2019. The red diamonds indicate the stations of LFM_LMS and the green rectangular represents the position of rocket-triggered lightning site. The purple cross indicates the first located source. The colors from blue to red indicate the time variation from the beginning to the end.

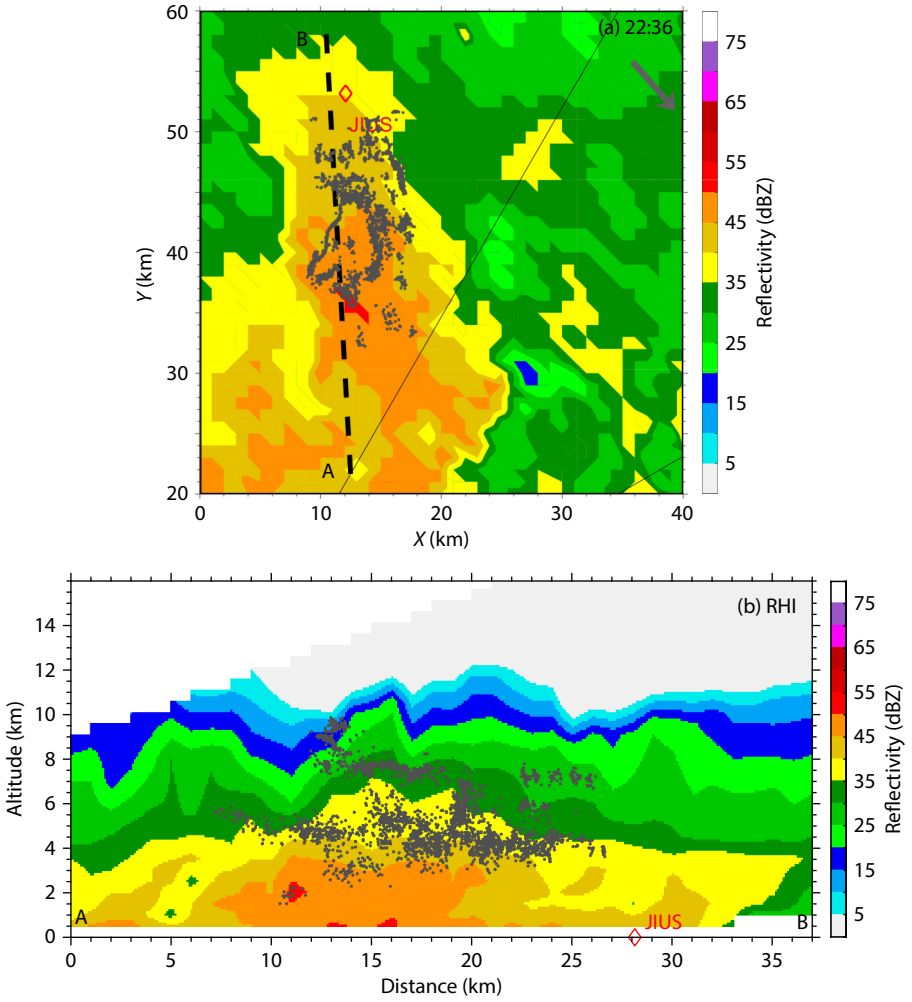

Figure 8. Composite radar reflectivity overlapped with the lightning radiation sources (upper panel a) and the range height indicator along the black dotted line AB (lower panel b). The black arrow indicates the moving direction of the thunderstorm.

From the location results, it can be found that the lightning starts from the top of the thundercloud by a downward preliminary leader at a height of 9.6 km above the ground level, which moves down to the southwest at a vertical speed of 1.44×10^6 m/s and then wraps back to the northeast horizontally at an altitude of about 7.4 km (as shown in Figure 7 and Figure S1). Subsequently, the leader continued to develop downward at a vertical speed of 5.03×10^5 m/s, a speed consistent with previous studies by VHF mapping system (Proctor, 1981; Shao XM and Krehbiel, 1996) and by high speed video (Fan XP et al., 2018), from an altitude of 6.8 to 3.7 km, and extend the lightning channels in the south area at about 3–5 km with reflectivity > 35 dBZ but < 45 dBZ (Figure 8). The scattered sources indicate that the lightning channels are more branching and complicated in this area. Notably, the propagation speed and the convergent radiation sources implied the preliminary downward leader with negative polarity (Qie XS et al., 2019). In addition, the *E*-field change (black solid line in Figure 7a) on the ground recorded at LIYA station (the distance is over 15 km far from the lightning occurrence position) also indicated the negative leader propagation at this stage because there was a declining change in the *E*-field waveform when the leader went far away from LIYA station.

Approximately 72.6 ms after the preliminary leader initiation, sources of the discharges were located to expand from south to north along the existing channels and continue to the northern part of the cloud at an altitude of 4–6 km. The *E*-field change at LIYA station indicates the propagation of the positive leader during this stage (a decreasing change corresponding to the nearing propagation leader). After that, the mapping results pointed out that the discharge continued in the north part and the channel elongated from west to east in the main layer with reflectivity > 35 dBZ at the height of ~4 km. According to the *E*-field change at LIYA station, the lightning channels are dominated by the negative leader. During the next 0.13 s, the scattered location sources in the north area show that the in-cloud discharges are in an extensive range. Thereafter, a dart negative leader propagated with an estimated speed of 1.68×10^6 m/s along the previously built channel in the south area, indicating a charge transfer between two different charge regions.

5. Conclusions

The LFM-LMS with a baseline of about 8–12 km has been developed during the SHAndong Triggered Lightning Experiment (SHATLE) since the summer campaign in 2016. The lightning

mapping system consists of 7 low-frequency magnetic field sensors, which received the magnetic radiations from lightning discharging processes at frequencies of 3 dB bandwidth in the range of 30–500 kHz and recorded the magnetic signal continuously and synchronously. Based on TDOA and a multi-grid nesting searching algorithm, magnetic signal pulses of lightning discharge are positioned with acceptable deviations. The Monte Carlo simulation results show that the accuracy within the location system is less than 200 m, and the location accuracy is more sensitive to the time difference than the altitude variation. The mean horizontal error is estimated to be 154 m, and the vertical error is estimated to be 205 m when referring to the initial upward leader in rocket-triggered lightning.

Further, the in-cloud channels of lightning are imaged, which proved the three-dimensional mapping capacity of LFM-LMS. The 3D morphology of a bipolar rocket-triggered lightning flash was constructed, and the beyond-visual-range discharge process and associated charge transfer are discussed. The 3D morphology of an unusual in-cloud lightning case was mapped by LFM-LMS. The propagation of the initial downward negative leader with a speed range of 0.5 to 1.4 × 10^6 m/s was depicted in this case, and the subsequent discharge in clouds is located during the entire active stage. The mapping results show that the continuous propagation path developed by the negative leader could be detected more distinctively than that of positive leaders. Meanwhile, the discharge position and the polarity of the in-cloud leaders in the propagation stage contribute to the determination of the polarity of the charge region, and further facilitate the study of the charge structure of the thundercloud.

Conclusively, the LFM-LMS in North China could reconstruct the in-cloud 3D morphology of the lightning and give more detailed information about lightning discharges, such as the onset altitude, the leader propagation speed, and even the development spatio-temporal scales. Meanwhile, this lightning mapping method facilitated the research on the special links between the discharge behaviors and the convection intensity of the thundercloud. Furthermore, another two LFM-LMS systems are also built in the TAIHU lake area (Jiangsu province) and Guangzhou Tower (Guangdong province), respectively. The three lightning location systems in China will play important roles in the research of the lightning activity in the plains of northern China, the lake's underlying surface, and urban buildings.

Data Availability Statement

All the data used for the analyses in this paper are available from https://zenodo.org/deposit/7874747; further information is available upon request from Gaopeng Lu (gaopenglu@gmail.com).

Acknowledgments

We would like to express our gratitude to colleagues participating in the summer observation campaign of SHATLE. This work was supported by the National Key R&D Program of China (2017YFC1501501), the CAS Project of Stable Support for Youth Team in Basic Research Field (YSRR-018), the Youth Innovation Fund project of the university (WK2080000172), the National Natural Science Foundation of China (41875006, U1938115), the Chinese Meridian Project, and the International Partnership Program of Chinese Academy of Sciences (183311KYSB20200003).

Supplementary Materials

S1. Mapping results of the natural lightning in four stages

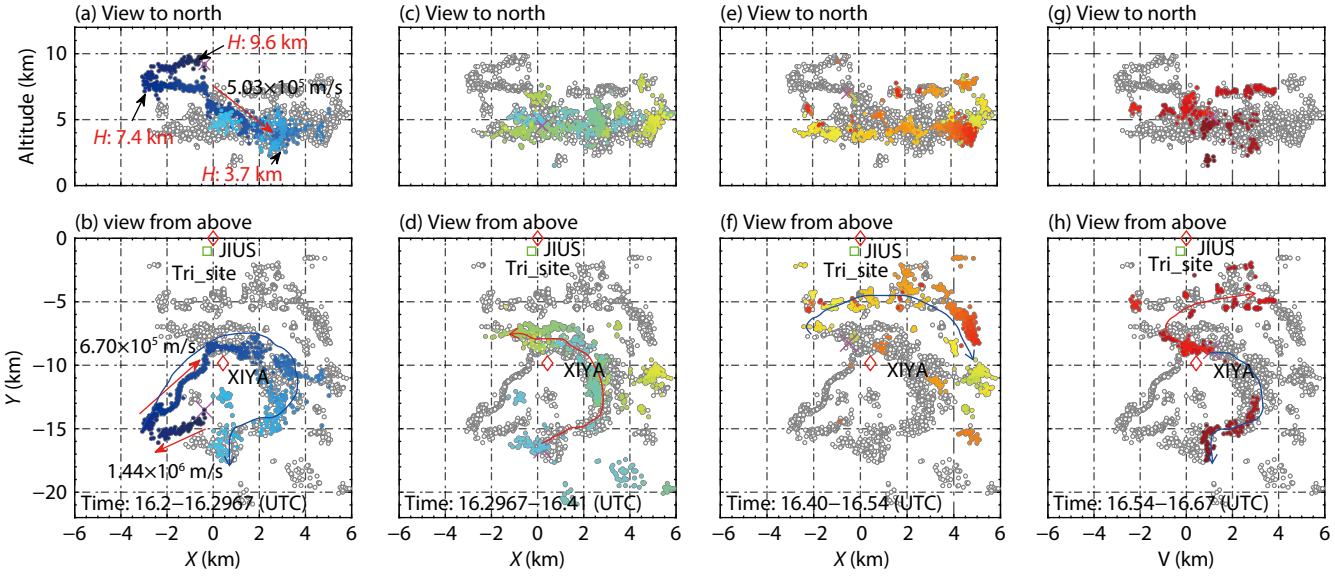

Figure S1. Mapping results of the lightning radiations in four stages. Vertical view of the flash from south to north are shown in (a), (c), (e) and (g). Plan view of the flash are shown in (b), (d), (f) and (h), respectively. Note that the blue-line arrow denotes the negative leader propagation and the red-line arrow denotes the positive leader propagation.

References

Bitzer, P. M., Christian, H. J., Stewart, M., Burchfield, J., Podgorny, S., Corredor, D., Hall, J., Kuznetsov, E., and Franklin, V. (2013). Characterization and applications of VLF/LF source locations from lightning using the Huntsville Alabama Marx Meter Array. *J. Geophys. Res.: Atmos.*, *118*(8), 3120–3138. https://doi.org/10.1002/jgrd.50271

Chen, Z. F., Zhang, Y., Zheng, D., Zhang, Y. J., Fan, X. P., Fan, Y. F., Xu, L. T., and Lyu, W. T. (2019). A method of three-dimensional location for LFEDA combining the time of arrival method and the time reversal technique. *J. Geophys. Res.: Atmos.*, *124*(12), 6484–6500. https://doi.org/10.1029/2019jd030401

Cummins, K. L., Murphy, M. J., Bardo, E. A., Hiscox, W. L., Pyle, R., and Pifer, A. E. (1998). Combined TOA/MDF technology upgrade of U.S. National Lightning Detection Network. *J. Geophys. Res.*, *103*, 9035–9044. https://doi.org/10.1029/98JD00153

Fan, X. P., Zhang, Y. J., Zheng, D., Zhang, Y., Lyu, W. T., Liu, H. Y., and Xu, L. T. (2018). A new method of three-dimensional location for low-frequency electric field detection array. *J. Geophys. Res.: Atmospheres*, *123*, 8792–8812. https://doi.org/10.1029/2017JD028249

Hare, B. M., Scholten, O., Bonardi, A., Buitink, S., Corstanje, A., Ebert, U., Falcke, H., Hörandel, J. R., Leijnse, H., … Winchen, T. (2018). LOFAR lightning imaging: Mapping lightning with nanosecond precision. *J. Geophys. Res.: Atmos.*, *123*(5), 2861–2876. https://doi.org/10.1002/2017JD028132

Karunarathne, S., Marshall, T. C., Stolzenburg, M., Karunarathna, N., Vickers, L. E., Warner, T. A., and Orville, R. E. (2013). Locating initial breakdown pulses using electric field change network. *J. Geophys. Res.: Atmos.*, *118*(13), 7129–7141. https://doi.org/10.1002/jgrd.50441

Koshak, W. J., Solakiewicz, R. J., Blakeslee, R. J., Goodman, S. J., Christian, H. J., Hall, J. M., Bailey, J. C., Krider, E. P., Bateman, M. G., and Cecil, D. J. (2004). North Alabama Lightning Mapping Array (LMA): VHF source retrieval algorithm and error analyses. *J. Atmos. Ocean. Technol.*, *21*(4), 543–558. https://doi.org/10.1175/1520-0426(2004)021<0543:NALMAL>2.0.CO;2

Li, F. Q., Sun, Z. L., Jiang, R. B., Tang, G. Y., Liu, M. Y., Li, X., Zhang, H. B., Yuan, S. F., Tian, Y., and Qie, X. S. (2021). A rocket-triggered lightning flash containing negative-positive-negative current polarity reversal during its initial stage. *J. Geophys. Res.: Atmos.*, *126*(9), e2020JD033187. https://doi.org/10.1029/2020JD033187

Liu, B., Shi, L. H., Qiu, S., Liu, H. Y., Dong, W. S., Li, Y., and Sun, Z. (2020). Fine three-dimensional VHF lightning mapping using waveform cross-correlation TOA method. *Earth Space Sci.*, *7*(1), e2019EA000832. https://doi.org/10.1029/2019EA000832

Lyu, F. C., Cummer, S. A., Solanki, R., Weinert, J., McTague, L., Katko, A., Barrett, J., Zigoneanu, L., Xie, Y. B., and Wang, W. Q. (2014). A low-frequency near-field interferometric-TOA 3-D lightning mapping array. *Geophys. Res. Lett.*, *41*(22), 7777–7784. https://doi.org/10.1002/2014GL061963

Lyu, F. C., Cummer, S. A., Lu, G. P., Zhou, X., and Weinert, J. (2016). Imaging lightning intracloud initial stepped leaders by low-frequency interferometric lightning mapping array. *Geophys. Res. Lett.*, *43*(10), 5516–5523. https://doi.org/10.1002/2016GL069267

Lyu, F. C., Cummer, S. A., Chen, M. L., Qin, Z. L., Lyu, W. T., and Sun, J. S. (2021). Three-dimensional mapping of two coincident flashes—An upward positive flash triggered by the in-cloud activity of a downward negative flash. *Atmos. Res.*, *250*, 105408. https://doi.org/10.1016/j.atmosres.2020.105408

Ma, Z. L., Jiang, R. B., Qie, X. S., Xing, H. Y., Liu, M. Y., Sun, Z. L., Qin, Z. L., Zhang, H. B., and Li, X. (2021). A low frequency 3D lightning mapping network in north China. *Atmos. Res.*, *249*, 105314. https://doi.org/10.1016/j.atmosres.2020.105314

Proctor, D. E. (1981). VHF radio pictures of cloud flashes. *J. Geophys. Res.*, *86*, 4041–4071. https://doi.org/10.1029/JC086iC05p04041

Proctor, D. E., Uytenbogaardt, R., and Meredith, B. M. (1988). VHF radio pictures of lightning flashes to ground. *J. Geophys. Res.*, *93*,12683–12727. https://doi.org/10.1029/JD093iD10p12683

Qie, X., Yang J., Jiang R., Wang J., and Liu D. (2010). A New-Model Rocket for Artificially Triggering Lightning and Its First Triggering Lightning Experiment. *Chinese Journal of Atmospheric Sciences* (in Chinese), *34*(5): 937–946.

Qie, X. S., Yuan, S. F., Zhang, H. B., Jiang, R. B., Wu, Z. J., Liu, M. Y., Sun, Z. L., Pu, Y. J., Li, J. L., … Lu, G. P. (2019). Propagation of positive, negative, and recoil leaders in upward lightning flashes. *Earth Planet. Phys.*, *3*(2), 102–110. https://doi.org/10.26464/epp2019014

Rhodes, C. T., Shao, X. M., Krehbiel, P. R., Thomas, R. J., and Hayenga, C. O. (1994). Observations of lightning phenomena using radio interferometry. *J. Geophys. Res.*, *99*(D6), 13059–13082. https://doi.org/10.1029/94JD00318

Rison, W., Thomas, R. J., Krehbiel, P. R., Hamlin, T., and Harlin, J. (1999). A GPS-based three-dimensional lightning mapping system: Initial observations in central New Mexico. *Geophys. Res. Lett.*, *26*(23), 3573-3576. 3573–3576. https://doi.org/10.1029/1999GL010856

Rakov, V. A., and Uman, M. A. (2003). Lightning: Physics and Effects. Cambridge Univ Press, New York.

Shao, X. M., and Krehbiel, P. R. (1996). The spatial and temporal development of intracloud lightning. *J. Geophys. Res.*, *101*(D21), 26641–26668. https://doi.org/10.1029/96JD01803

Shao, X. M., Krehbiel, P. R., Thomas, R. J., and Rison, W. (1995). Radio interferometric observations of cloud-to-ground lightning phenomena in Florida. *J. Geophys. Res.*, *100*(D2), 2749–2783. https://doi.org/10.1029/94JD01943

Shi, D. D., Zheng, D., Zhang, Y., Zhang, Y. J., Huang, Z. G., Lu, W. T., Chen, S. D., and Yan, X. (2017). Low-frequency E-field detection array (LFEDA)—Construction and preliminary results. *Sci. China Earth Sci.*, *60*(10), 1896–1908. https://doi.org/10.1007/s11430-016-9093-9

Smith, D. A., Eack, K. B., Harlin, J., Heavner, M. J., Jacobson, A. R., Massey, R. S., Shao, X. M., and Wiens, K. C. (2002). The Los Alamos Sferic Array: A research tool for lightning investigations. *J. Geophys. Res.*, *107*(D13), 4183. https://doi.org/10.1029/2001JD000502

Smith, D. A., Heavner, M. J., Jacobson, A. R., Shao, X. M., Massey, R. S., Sheldon, R. J., and Wiens, K. C. (2004). A method for determining intracloud lightning and ionospheric heights from VLF/LF electric field records. *Radio Sci.*, *39*(1), RS1010. https://doi.org/10.1029/2002RS002790

Stock, M. G., Akita, M., Krehbiel, P. R., Rison, W., Edens, H. E., Kawasaki, Z., and Stanley M. A. (2014). Continuous broadband digital interferometry of lightning using a generalized cross-correlation algorithm. *J. Geophys. Res.: Atmos.*, *119*, 3134–3165. https://doi.org/10.1002/2013JD020217

Thomas, R., Krehbiel, P., Rison, W., Hunyady, S., Winn, W., Hamlin, T., and Harlin, J. (2004). Accuracy of the lightning mapping array. *J. Geophys. Res.*, *109*, D14207. https://doi.org/10.1029/2004JD004549

Wang, Y., Qie, X. S., Wang, D. F., Liu, M. Y., Su, D. B., Wang, Z. C., Liu, D. X., Wu, Z. J., Sun, Z. L., and Tian, Y. (2016). Beijing Lightning Network (BLNET) and the observation on preliminary breakdown processes. *Atmos. Res.*, *171*, 121–132. https://doi.org/10.1016/j.atmosres.2015.12.012

Wang, Y. P., Lu, G. P., Ma, M., Zhang, H. B., Fan, Y. F., Liu, G. J., Wan, Z. R., Wang, Y., Peng, K. M., … and Zhou, R. X. (2019). Triangulation of red sprites observed above a mesoscale convective system in North China. *Earth Planet. Phys.*, *3*(2), 111–125. https://doi.org/10.26464/epp2019015

Wu, T., Wang, D. H., and Takagi, N. (2018). Lightning mapping with an array of fast antennas. *Geophys. Res. Lett.*, *45*(8), 3698–3705. https://doi.org/10.1002/2018GL077628

Yoshida, S., Wu, T., Ushio, T., Kusunoki, K., and Nakamura, Y. (2014). Initial results of LF sensor network for lightning observation and characteristics of lightning emission in LF band. *J. Geophys. Res.: Atmospheres*, *119*, 12034–12051. https://doi.org/10.1002/2014JD022065

Yang, Q. L., Wang, J. Q., Zhou, X., Yuan, S. B., Meng, X. Y., Xiao, F., Jin, H. L., Xue, W. Q., and Ma, Q. M. (2021). Preliminary evaluation of Hai-Nan Lightning Detection Network (HNLDN). *Radio Sci.*, *56*(9), e2021RS007321. https://doi.org/10.1029/2021RS007321

Yi, J., Gu, X. D., Cheng, W., Tang, X. Y., Chen, L., Ni, B. B., Zhou, R. X., Zhao, Z. Y., Wang, Q., and Zhou, L. Q. (2020). A detailed investigation of low latitude tweek atmospherics observed by the WHU ELF/VLF receiver: 2. Occurrence features and associated ionospheric parameters. *Earth Planet. Phys.*, *4*(3), 238–245. https://doi.org/10.26464/epp2020023

Yuan, S. F., Qie, X. S., Jiang, R. B., Wang, D. F., Sun, Z. L., Srivastava, A., and Williams, E. (2020). Origin of an uncommon multiple-stroke positive cloud-to-ground lightning flash with different terminations. *J. Geophys. Res.: Atmos.*, *125*(15), e2019JD032098. https://doi.org/10.1029/2019JD032098

Zhang, G. S., Li, Y. J., Wang, Y. H., Zhang, T., Wu, B., and Liu, Y. X. (2015). Experimental study on location accuracy of a 3D vhf lightning-radiation-source locating network. *Sci. China Earth Sci.*, *58*(11), 2034–2048. https://doi.org/10.1007/s11430-015-5119-1